Supporting Information

Unique photo-chemo-immuno-nanoplatform against orthotopic xenograft oral cancer and metastatic syngeneic breast cancer

Lu Zhang[†,#], Di Jing[†,⊥,#], Lei Wang[‡], Yuan Sun[†], Jian Jian Li[//], Brianna Hill[†], Fan Yang[†], Yuanpei Li[†], Kit S Lam[†*]*

[†]Department of Biochemistry and Molecular Medicine, UC Davis NCI-designated Comprehensive Cancer Center, University of California Davis, Sacramento, California, 95817, USA.

[‡]CAS Center for Excellence in Nanoscience, CAS Key Laboratory for Biomedical Effects of Nanomaterials and Nanosafety, National Center for Nanoscience and Technology, Beijing 100190, China.

[//] Director of Translational Research, Department of Radiation Oncology, School of Medicine, University of California Davis, Sacramento, California, 95817, USA.

[⊥]Department of Oncology, Xiangya Hospital, Central South University, Hunan, 410008, China.

Corresponding Authors

*E-mail: kslam@ucdavis.edu. Tel: (916)734-0910.

*E-mail: lypli@ucdavis.edu. Tel: (916)7344420. Fax: (916)7346415.

Materials and Methods

Monomethylterminated poly(ethylene glycol) monoamine (MeO-PEG-NH_2, Mw ≈ 5000 Da) was purchased from Rapp Polymere (Germany). 4-Carboxyphenylboronic acid, 4-Carboxyphenylboronic acid pinacol ester, 3-Carboxy-5-nitrophenylboronic acid and 3-Carboxy-5-nitrophenylboronic acid pinacol ester were obtained from Combi-Blocks (San Diego, CA). (Fmoc)Lys(Boc)-OH, (Fmoc)Lys(Fmoc)-OH, (Fmoc)Cys(Trt)-OH and (Fmoc)Ebes-COOH were purchased from AnaSpec Inc. (San Jose, CA). All other chemicals were purchased from Sigma-Aldrich (St. Louis).

Synthesis of indocyanine green derivative (ICGD)

Briefly, 1,1,2-trimethylbenz[e]indole (I) and iodoethane (1.5 eq) reacted in acetonitrile solution under 90 °C heating and refluxed for 3 days. After that, ether was added to produce 3-ethyl-1,1,2-trimethyl-1H-benzo[e]indol-3-ium (II). Then crude produce (II) was added to N-[5-(phenylamino)-2,4-pentadienylidene]aniline monohydrochloride (1 eq) in acetic anhydride. The mixture was heated to 100 °C for 1.5 h, cooled to room temperature, and added to deionized water. After filtered, produce (III) 3-ethyl-1,1-dimethyl-2((1E,3E,5E)-6-(N-phenylacetamido)hexa-1,3,5-trien-1-y1)-1H-benzo[e]in dol-3-ium was got. In addition, 1,1,2-trimethylbenz[e]indole (I) and 5-bromovaleric acid of potassium iodide (1.2 eq) reacted in acetonitrile solution under 100 °C heating and refluxed for 5 days. After that, ether was added to produce 3-(4-carboxybutyl)-1,1,2-trimethyl-1H-benzo[e]ondol-3-ium (IV). Finally, crude IV was added

into III of pyridine. The mixture was heated for 30 min at 40 °C and concentrated in vacuo to get final produce. The final crude produce was purified *via* silicagel column twice to get ICGD.

Synthesis of telodendrimers

The first representative ICGD/CA telodendrimer (PEG_{5k}-$ICGD_4$-CA_4, abbreviated as PIC) was synthesized *via* solution-phase condensation reactions from MeO-PEG-NH_2 utilizing stepwise peptide chemistry according to our published methods.[30] Briefly, (Fmoc)Lys(Fmoc)-OH (3 eq) was coupled on the NH_2 terminus of PEG using DIC and HOBt as coupling reagents until a negative Kaiser test result was obtained, thereby indicating completion of the coupling reaction. PEGylated molecules were precipitated by adding cold ether and then washed with cold ether twice. Fmoc groups were removed by the treatment with 20% (v/v) 4-methylpiperidine in dimethylformamide (DMF), and the PEGylated molecules were precipitated and washed three times by cold ether. White powder precipitate was dried under vacuum and one coupling of (Fmoc)Lys(Fmoc)-OH and one coupling of (Fmoc)lys(Boc)-OH were carried out, respectively, to generate a third generation of dendritic polylysine terminated with four Boc and Fmoc groups on one end of PEG. Boc groups were removed firstly by 50% (v/v) trifluoroacetic acid in dichloromethane, and CA NHS esters were coupled to the terminal end of dendritic polylysine. After that, Fmoc protecting groups were removed by 20% (v/v) 4-methylpiperidine in dichloromethane, and then ICGD was coupled to the terminal end of dendritic polylysine. The telodendrimer solution was filtered and then dialysed against water with MWCO of 3.5 KDa. Finally, the PIC telodendrimer was lyophilized.

The second thiolated telodendrimer (named as PEG_{5k}-Cys_4-L_8-CA_8, abbreviated as PCLC) was synthesized according to our previously report. Briefly, a third generation of dendritic polylysine terminated with four Boc and Fmoc groups on one end of PEG firstly was synthesized following the above method. After the removal of Boc groups with 50% (v/v) trifluoroacetic acid (TFA) in dichloromethane (DCM), (Fmoc)Cys(Trt)eOH, (Fmoc)Ebes-OH and Cholic acid NHS esterwere coupled step by step to the terminal end of dendritic polylysine. The Trt groups on cysteines were removed by TFA/H2O/ethanedithiol (EDT)/triethylsilane (TIS) (94:2.5:2.5:1, v/v) resulting in PCLC thiolated telodendrimer. The thiolated telodendrimer was recovered from the mixture by three cycles of dissolution/reprecipitation with DMF and ether, respectively. Finally, the thiolated telodendrimer was dissolved in acetonitrile/water and lyophilized.

The molecular weight of PIC and PCLC telodendrimers were collected on ABI 4700 MALDI-TOF/TOF mass spectrometer (linear mode) using R-cyano-4-hydroxycinnamic acid as a matrix. The monodispersed mass traces were detected for the telodendrimers, and the molecular weight of the telodendrimer from MALDI-TOF MS was almost identical to the theoretical value. ^{1}H NMR spectra of the telodendrimers were recorded on an Avance 600 Nuclear Magnetic Resonance Spectrometer (Bruker) using $CDCl_3$ as solvents.

Preparation of CPCI-NP

10 mg PIC telodendrimer was dissolved in 1 mL PBS followed by sonication for 10 min to form PIC NPs. In order to make CPIC NPs, 10 mg PCLC telodendrimer and 10 mg PCI telodendrimer were dissolved in 1mL PBS to form micelles and then sonicated for 10 min. The thiol groups on

the telodendrimer were oxidized to form disulphide linkages by air.

Preparation of CPCI/DOX-NP and CPCI/Imiquimod-NP

Hydrophobic drugs, such as DOX or imiquimod, were loaded into CPIC NPs by the solvent evaporation method. Before the encapsulation of DOX into NPs, DOX•HCl was stirred with 3 molar equivalent of triethylamine in chloroform ($CHCl_3$)/methanol (MeOH; 1:1, v/v). In all, 10 mg PCI telodendrimer and 10 mg PCLC telodendrimer along with different amounts of DOX were first dissolved in $CHCl_3$/MeOH, mixed and evaporated on rotavapor to obtain a homogeneous dry polymer film. The film was reconstituted in 1mL PBS, followed by sonication for 30 min, allowing the sample film to disperse into nanoparticles solution. Finally, the nanoparticles solution was filtered with a 0.22-mm filter to sterilize the sample. The imiquimod-loaded CPIC NPs were prepared *via* the similar method except without 3 molar equivalent of triethylamine.

Characterizations of nanoparticles

The size and size distribution of nanoparticles were measured by DLS instruments (Microtrac, USA). The concentrations were kept at 1.0 mg mL^{-1} for DLS measurements. The data are presented as the mean ± standard deviation. The morphology of nanoparticles was observed on a Philips CM-120 TEM. Briefly, A 5 μL amount of a sample solution (1.0 mg mL^{-1}) was dried at room temperature on the copper grid. Uranyl acetate solution (2 wt % in water) was added to negatively stain the sample for 30 s and then blotted off using filter paper. The grid was dried overnight before TEM analysis. UV-vis-NIR absorption and fluorescence spectra of NPs were

measured by Genesys 10S UV-Vis spectrophotometer (Thermo Scientific, Waltham, MA).

Stability of nanoparticles in SDS and human plasma

The stability study was performed to monitor the change in fluorescence and particle size of PCI-NP and CPCI-NP in the presence of SDS, which was reported to be able to efficiently break down polymeric micelles. An SDS solution (7.5 mg mL^{-1}) was added to aqueous solutions of nanoparticles (1.5 mg mL^{-1}). The final SDS concentration was 2.5 mg mL^{-1} and the micelle concentration was kept at 1.0 mg mL^{-1}. The fluorescence signal of the solutions was measured by fluorescence spectrometer. The size and size distribution of the nanoparticles were monitored at predetermined time intervals by DLS. The stability of the micelles was also evaluated in the presence of GSH (10 mM) together with SDS. The stability of DOX-loading CPCI/DOX-NP was further studied in 10 % (v/v) plasma from healthy human volunteers. The mixture was incubated at physiological body temperature (37 °C) followed by size measurements at predetermined time intervals up to 96 h.

Photothermal effect of nanoparticles

1 mL of PCI-NP, CPCI-NP and polyethylene glycol (PEG) coated gold nanorod (GNRs) was added into a 4 mL transparent quartz vial, respectively. The solution was irradiated with a fiber-coupled continuous semiconductor diode laser (808 nm, Beijing Viasho Technology Co., Ltd., China). The power density was 0.8 W cm^{-2}, and the temperature was monitored with a thermal infrared imaging camera (Flir C2, USA). To study the photostability of CPCI-NP, 1 mL of CPCI-NP, PCI-NP, ICG aqueous solution and CPCI-NP aqueous solution with GSH and SDS

(were irradiated with 808 nm laser for 5 min and then cooled down to the room temperature. The heating and cooling were repeated five times to test the photothermal stability. The calculation method of photothermal conversion efficiencies was demonstrated in the supplementary information.

***In vitro* Photothermal Studies**

From an energy balance in a system, we can describe the total energy balance as:

$$\sum_i m_i C_{p,i} \frac{dT}{dt} = Q_{in,np} + Q_{in,surr} - Q_{out} \quad (1)$$

Where *m*, *Cp* and *T* are the mass of the solvent, the heat capacity of the solvent and the solution temperature, respectively. $Q_{in,np}$ is the photothermal energy input from the nanoparticles, which can be described as:

$$Q_{in,np} = I\left(1 - 10^{(-A_\lambda)}\right)\eta \quad (2)$$

Where *I* is the laser power used for the photothermal experiment. $A\lambda$ is the absorbance at the used laser wavelength (808 nm), and η is the photothermal transduction efficiency.

$Q_{in,surr}$ stands for the heat input due to light absorption by the solvent and container, which can be determined by:

$$Q_{in,surr} = Q_{Dis} = hS_{buff} \times (T_{Max} - T_{Surr})_{buff} \quad (3)$$

Where hS_{buff} is the parameter relevant with container and solvent (*h* and *S* stand for heat transfer coefficient and surface area of the container, respectively). T_{Max} is the maximum steady-state temperature of solvent. T_{Surr} is the ambient surrounding temperature. Q_{out} is the heat lost to the surrounding:

$$Q_{out} = hS \times (T - T_{surr}) \quad (4)$$

hS can be determined by measuring the rate of temperature decrease after removing the light source. In the absence of any laser excitation, combining eq. (4) with eq. (1) yields

$$\sum_i m_i C_{p,i} \frac{dT}{dt} = - Q_{out} = - hS \times (T - T_{surr}) \quad (5)$$

After rearrangement and integration, the following expression for *t* is obtained:

$$t = - \left(\frac{m_{buff} \times C_{p,buff}}{hS}\right) \ln\left(\frac{T - T_{surr}}{T_{max} - T_{surr}}\right) \quad (6)$$

Two characteristic rate constants can then be defined, $\tau_s = \frac{m_{buff} \times C_{p,buff}}{hS}$, $\theta = \frac{T - T_{surr}}{T_{max} - T_{surr}}$, such that:

$$t = - \tau_s \ln(\theta) \quad (7)$$

According to the cooling curve, τ_s and heat transfer coefficients (*hS*) can be determined. The parameter hS_{buff} can be calculated in the same way, when container just contains buffer. At the maximum steady state temperature, eq (1) equals to 0 and we can get

$$Q_{in,np} + Q_{in,surr} = I\left(1 - 10^{(-A_\lambda)}\right)\eta + Q_{dis} = Q_{out} = hS \times (T_{max} - T_{surr}) \quad (8)$$

Where T_{max} is the maximum steady-state temperature. Therefore, the photothermal conversion efficiency can be calculated as

$$\eta = \frac{hS(T_{max} - T_{surr}) - Q_{dis}}{I\left(1 - 10^{(-A_\lambda)}\right)} \quad (9)$$

I is the laser power used for the photothermal experiment and A_{808} is the absorbance of the nanoparticle at 808 nm.

In vitro **penetration depth and thermal effect of nanoparticles**

To investigate the relationship of heating effect and tissue penetration depth of CPCI-NP under

laser irradiation at 808 nm, simulation experiment *in vitro* was first designed. This experiment was divided into two groups: (1) CPCI-NP and (2) PCLC/TBAI&ICG-NP. Group (2) was prepared by following method: the complex of free ICG and tetra-n-butylammonium iodide (TBAI) *via* electrostatic interactions could be physically encapsulated into PCLC toledendrimer, named as PCLC/TBAI&ICG NPs. Hotpot beef was chose as simulation tissue and cut into square pieces (thickness of each piece: 2 mm). 100 μL CPCI-NP (ICGD concentration at 30 μg mL^{-1}) or PCLC/TBAI&ICG-NP (ICG concentration: 30 μg mL^{-1}) solutions was dripped on the surface of beef and 808 nm laser (0.8 W cm^{-2}, 30s) was applied from the below of device. Temperature and beef piece thickness were recorded by thermal infrared camera.

DOX release from CPCI/DOX-NP

In vitro DOX release profiles from CPCI/DOX-NP were further measured by the dialysis method. The drug release experiment was divided into three groups: (1) PBS, (2) GSH (10 mM), (3) GSH (10 mM) with NIR irradiation (808 nm laser, 0.8 W cm^{-2}). First, 500 μL of CPCI/DOX-NP solution (with DOX concentration at 1 mg mL^{-1}) was transferred into a dialysis bag to dialyze against DI water. All groups were first evaluated for 4 h at 37 °C with shaking. After that, GSH was added into group (2). Group (3) added GSH and was irradiated under laser at 808 nm three times at appropriate time points. For all groups, 10 μL of solutions were taken out at desired time points, and then was added into one bottle with 90 μL DMSO. The released DOX content was analyzed on an HPLC system, wherein calibration curve was obtained using a series of drug/DMSO standard solutions with different concentrations. Data were reported as the average

percentage of DOX accumulative release for each triplicate sample.

***In vitro* cell experiments**

The *in vitro* cell cytotoxicity, cellular uptake study and combination therapy of samples were assessed on human OSC-3 oral cancer cell line, which was from Fan Yang's Lab. The cells were cultured with DMEM supplemented with 10% FBS and 1% Penicillin at 37 °C in humidified atmosphere with 5% CO_2 for 24 h. Then the samples were added to each well and the cells were incubated at 37 °C for an additional 24 h. To assess cellular uptake, OSC-3 cells were seeded into eight-well chamber slides at a density of 5×10^3 cells and incubated with CPCI/DOX-NP (DOX concentration: 25 μg mL^{-1}) for another 6 h. After DAPI staining for half an hour, cellular uptake was determined by confocal images. The relative cell viabilities were then measured by MTS assay. For *in vitro* chemo-/photothermal combination therapy, OSC-3 cells were seeded into 96-well plates (n = 3) and incubated with different samples for 12 h, followed by exposure to an 808 nm laser (0.8 W cm^{-2}, 2 min). Thereafter, the cells were incubated for another 24 h at 37 °C and MTS reagent was added into each well. The relative cell viabilities were then measured by Micro-plate reader (SpectraMax M2). Percentage of cell viability represents drug effect, and 100% means all cells survived. Cell viability was calculated using the following equation: Cell viability (%)=(OD490nm of treatment/OD490nm of blank control) × 100%. For *in vitro* cells apoptosis experiment, OSC-3 cells were co-cultured with different samples for 8h (DOX concentration: 25 μg mL^{-1} and 808 nm NIR laser with 0.8 W cm^{-2}, 2 min, if applied). Cells were washed two times and replaced with fresh medium. Then, cells were co-cultured with PI/Dio

FITC for 30min in a 12-well plate. Cell apoptosis was monitored utilizing fluorescence microscopy and Flow-cytometry. Representative FCM analysis scattergrams of PI/Annexin V showed apoptosis in the four groups.

***In vivo* blood elimination kinetics**

The jugular vein of female Sprague–Dawley rats was implanted with catheter for blood collection (Harland, Indianapolis, IN, USA). Free ICG, PCLC/TBAI&ICG NPs and CPCI-NP at identical ICG concentration were injected through the catheter at a dose of 5 mg kg $^{-1}$ body weight (n=3 for each group). All of the blood samples were collected from the catheter at different time point. Micro-plate reader (SpectraMax M2) was used to measure the ICG concentration at absorbance 808 nm.

Animal model

All animal experiments were in accordance with protocols No.19724, which was approved by the Animal Use and Care Administrative Advisory Committee at the University of California, Davis. Orthotopic OSC-3 oral cancer model: female nude mice were 6–8 weeks of age, which were purchased from Harlan (Livermore, CA, USA). The orthotopic oral cancer model was implanted in lip, which was the first time established. Each female nude mouse was implanted by injecting 1×10^6 OSC-3 oral cancer cells in 10 μL of PBS. 4T1 breast cancer model: Female Balb/c mice (8–10 weeks) were purchased from Harlan (Livermore, CA, USA). 4T1 cells (1×10^6) suspended in 80 μL mixture of PBS and Matrigel (1:1 v/v), then were injected into the forth breast fat pad.

***In vivo/Ex vivo* fluorescence imaging**

Nude mice bearing orthotopic OSC-3 oral cancer were subjected to tail vein injection of CPCI/DOX-NP at a dose of 7 mg ICGD per Kg body weight. Mice under ketamine anesthesia were imaged using *in vivo* fluorescence imaging system (Carestream In-Vivo Imaging System FX PRO, USA) at pre-designed time points. At 48 h after NPs injection, all animals were sacrificed, and their organs and tumor were excised for *ex vivo* imaging.

***In vivo* cancer treatment**

Orthotopic OSC-3 oral cancer tumor-bearing mice were injected with PBS, free DOX, PCI-NP, CPCI-NP, CPCI/DOX-NP. After 24 h and 48h, tumors were locally irradiated twice by laser (0.8 W cm^{-2} for 2 min) under general anaesthesia. Mice were treated once per week for two cycles. We used thermal camera (FLIR) to record tumor surface temperature. Mice bearing 4T1 tumor were randomly divided into seven groups for treatments with PBS, CPCI/Imi, CPCI+L, CPCI/Imi+L, CPCI/Imi+α-PD-1, CPCI/Imi+L+α-PD-1 and CPCI/Imi+L+α-PD-1 (1 cycle), respectively. Tumor sizes were measured twice a week and calculated using the following equation: volume = $0.5 \times L \times W^2$.

Real-time PCR

Three days after 1 cycle immune therapy, Blab/c mice were sacrificed and both sides of the tumor residue tissues were collected for assessment by RT-PCR. Tumor tissues added 1ml Trizol were dissolved by ultrasound and RNA was isolated using the Direct-zol™ R2071 kit. Fifty nanograms of total RNA from each specimen was reverse transcription cDNA using Lucigen kit. TNF-α,

IFN-γ, CD11b, IL-4, IL-6, IL-12 primary sequences of mice were prepared. PCR reactions were run on 96-well plates using Real Time PCR system (Applied Biosystems).

Histology studies

OSC-3 oral tumor-bearing mice were sacrificed after 1 cycle's treatment post-injection. Tumor tissues were fixed and embedded in paraffin. Haematoxylin and eosin (H&E) staining slides were prepared by BBC Biochemical (Mount Vernon, WA) and observed using microscopy.

Immunohistochemistry (IHC)

Tissue sections were processed for IHC using the following primary antibodies: a rat monoclonal to CD8 (eBioscience, antibody dilution 1:400), a rat monoclonal to CD4 (eBioscience, antibody dilution 1:200), a rabbit monoclonal to CD3 (abcam, antibody dilution 1:1000), a rabbit monoclonal to PD-1(abcam, antibody dilution 1:500), and a rabbit monoclonal to PD-L1(Cell Signaling, antibody dilution 1:200). All IHC was performed manually without the use of an automated immunostainer. Antigen retrieval was performed using a Decloaking Chamber (Biocare Medical, Concord, CA) with citrate buffer at pH 6.0 or Tris-EDTA at pH8.0, 125°C and pressure to 15 psi. Incubation with the primary antibody was performed at room temperature overnight in a humidified chamber. Normal goat serum was used for blocking. Biotinylated goat anti-rabbit (1:1000; Vector Labs, Burlingame, CA) was the secondary antibody used with a Vectastain ABC Kit Elite and a Peroxidase Substrate Kit DAB (both from Vector Labs) used for amplification and visualization of signal, respectively.

Statistical analysis

All the data were presented as mean ± s.d.. Unpaired student's *t*-test (two-tailed) was used for comparison between two groups. One-way analysis of variance (ANOVA) was used for multiple-group analysis. Statistical significance was set at $*p < 0.05$, $**p < 0.01$, $***p < 0.001$. All statistical tests were two-sided.

Supporting Figures

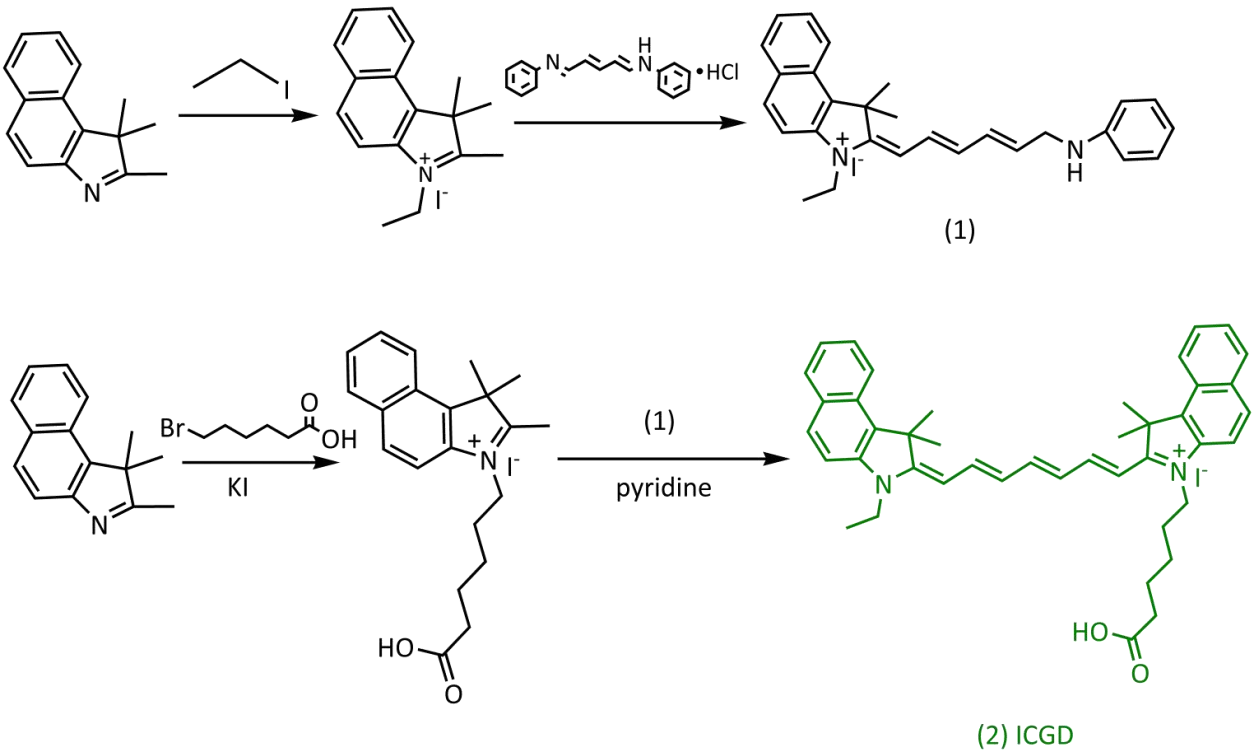

Figure S1. Synthetic approach of ICGD *via* multi steps chemical reactions.

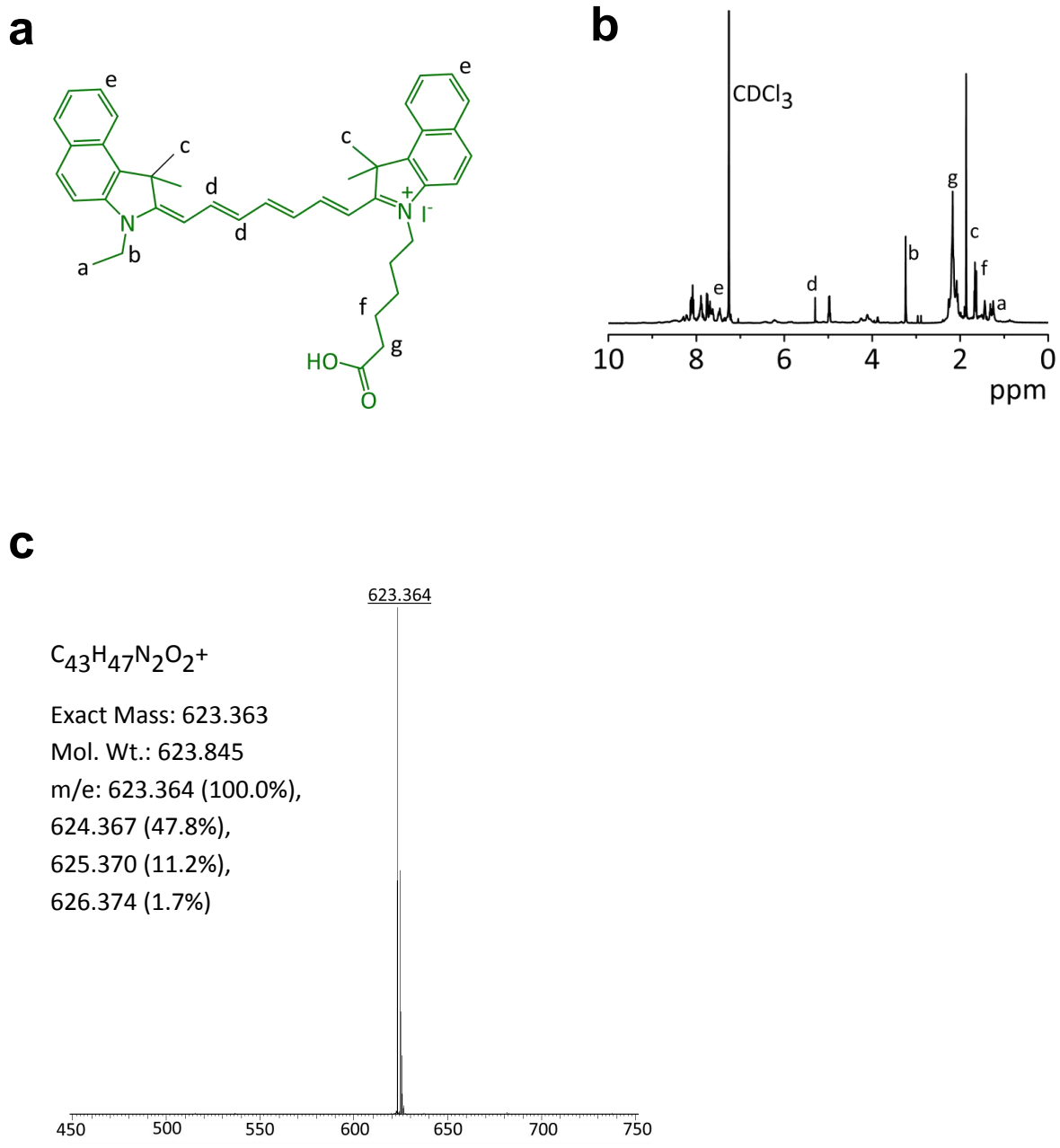

Figure S2. Chemical characterization of ICGD molecule. (a) Chemical structure, (b) ^{1}H NMR spectra in $CDCl_3$, (c) mass spectra *via* ESI of ICGD molecule.

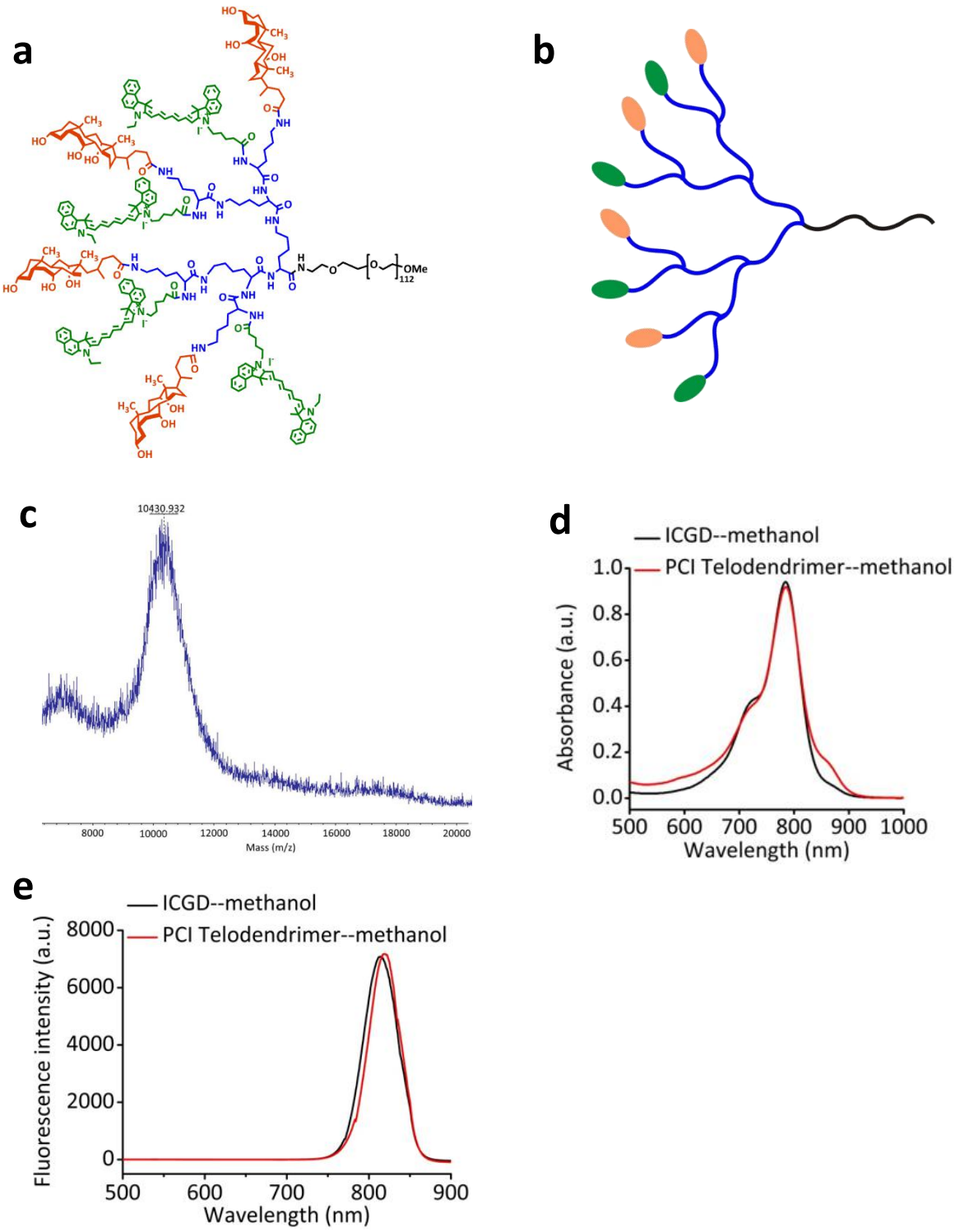

Figure S3. Chemical characterization of PCI telodendrimer. (a) Chemical structure, (b) schematic illustration, (c) mass spectra *via* MALDI-TOF of PCI telodendrimer. (d) UV–vis–NIR absorption spectra and (e) fluorescence spectra of ICGD molecule and PCI telodendrimer in methanol.

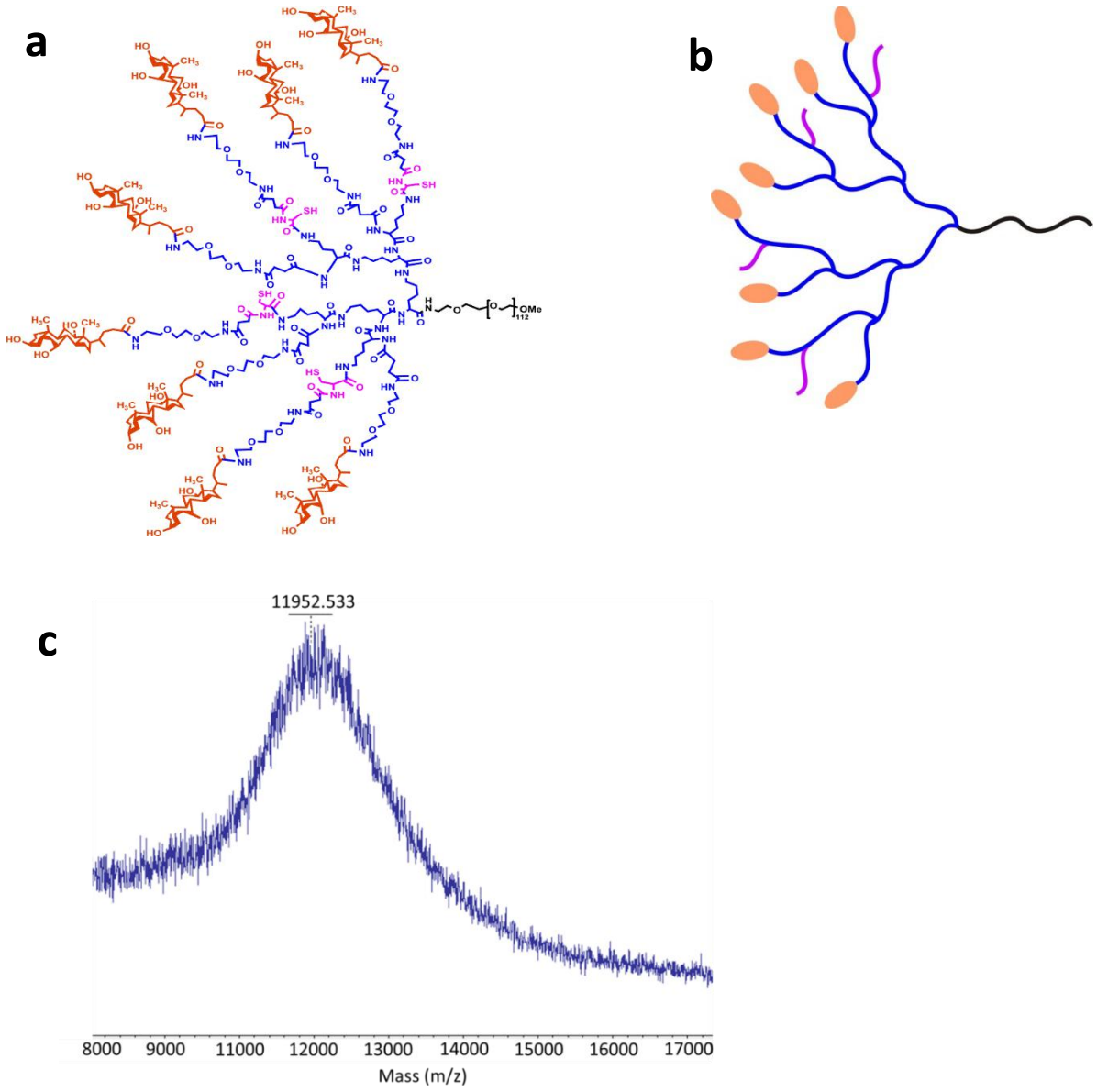

Figure S4. Chemical characterization of PCLC telodendrimer. (a) Chemical structure, (b) schematic illustration, (c) mass spectra *via* MALDI-TOF of PCLC telodendrimer.

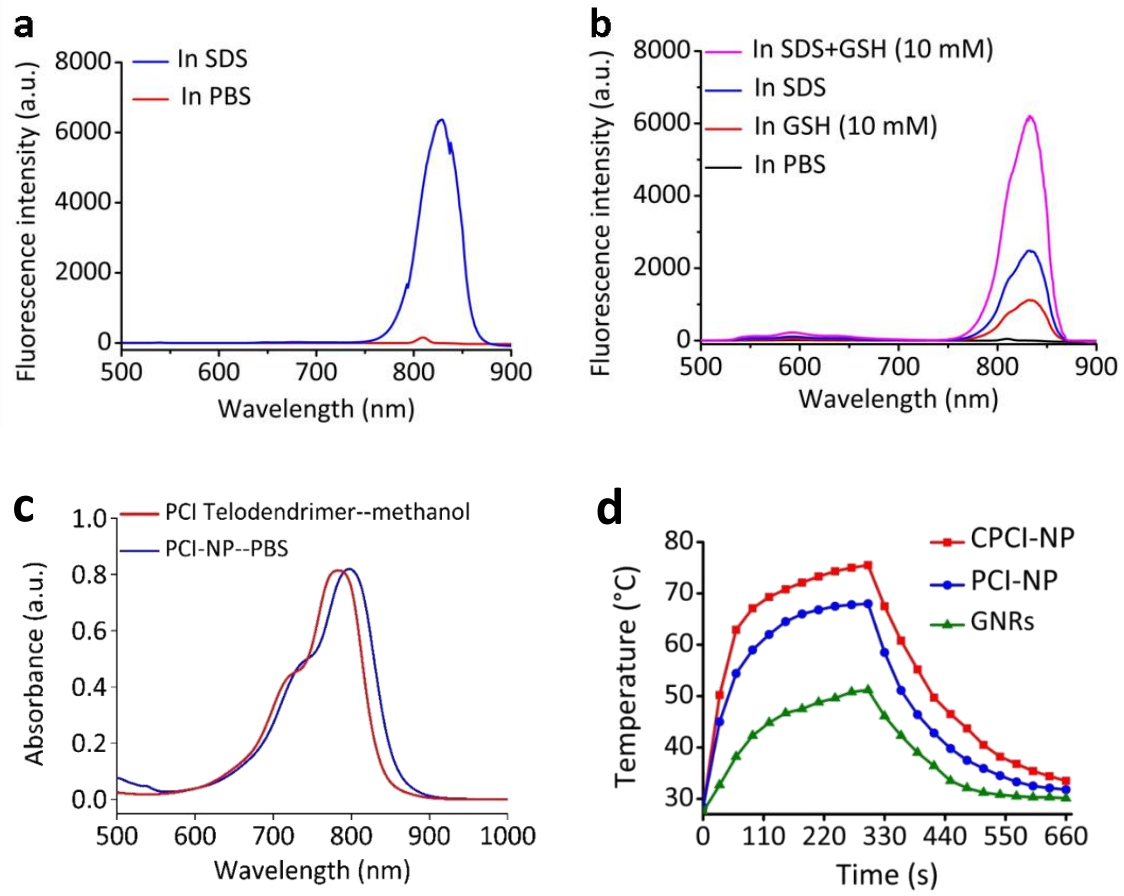

Figure S5. (a) Fluorescence spectra of ICGD from PCI-NP in PBS and SDS (PCI telodendrimer concentration: 0.1 mg mL^{-1}). (b) Fluorescence spectra of ICGD from CPCI-NP in PBS, SDS, GSH and GSH+ SDS (PCI telodendrimer concentration: 0.1 mg mL^{-1}). (c) UV–vis–NIR absorption spectra of PCI telodendrimer in methanol and PCI-NP in PBS. (d) Comparison of the photothermal conversion behavior of CPCI NPs, PCI NPs, and GNRs under laser irradiation at 808 nm for 300 s (ICGD concentration: 30 μg mL^{-1}, GNRs concentration: 18 μg mL^{-1}).

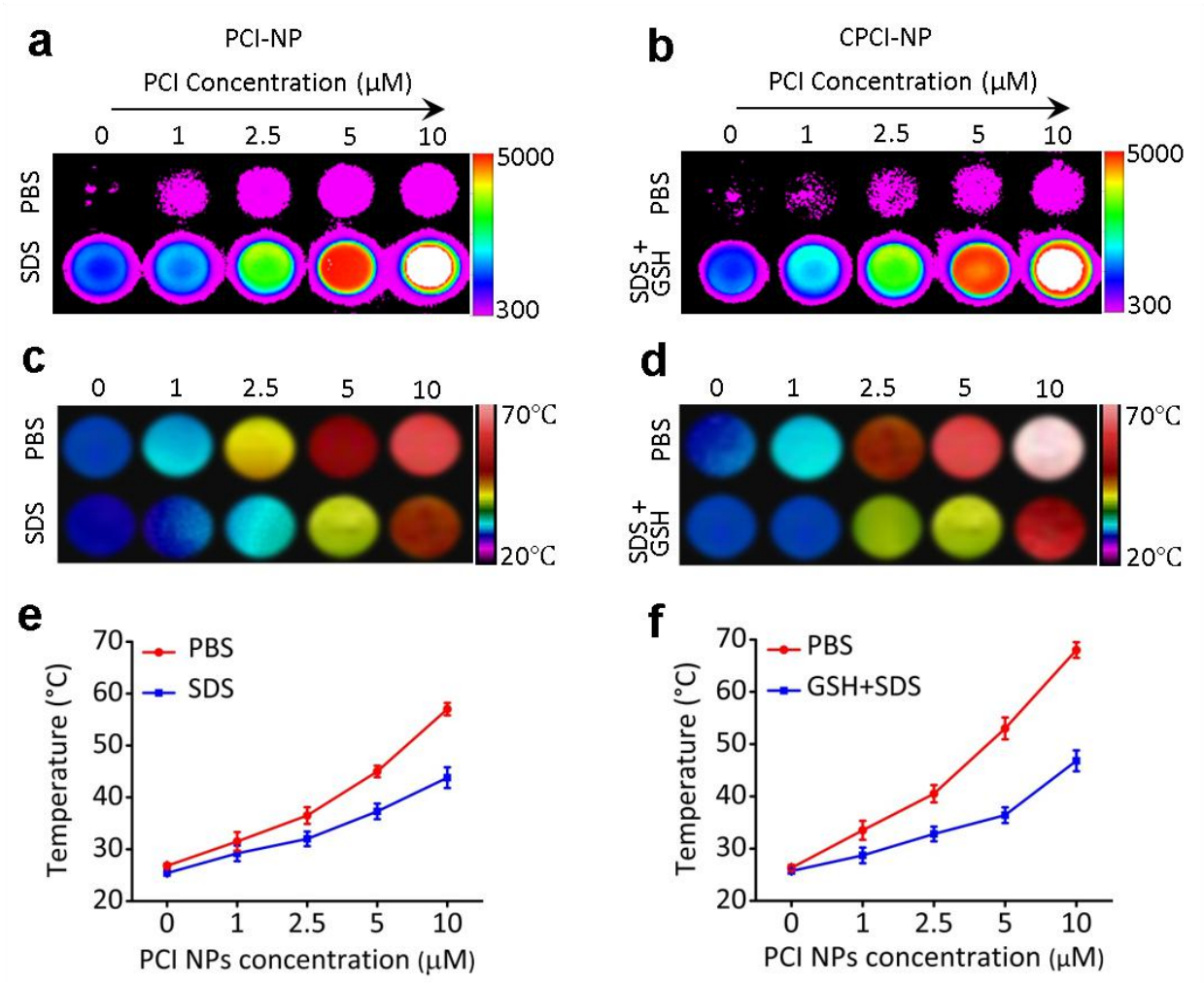

Figure S6. Mechanism analysis of CPCI-NP with high photothermal conversion efficiency. Near-infrared fluorescence imaging of (a) PCI-NP and (b) CPCI-NP solution (10 μL) in the absence and in the presence of SDS or GSH+SDS at the different concentration. Thermal images and quantitative temperature change curves of PCI-NP (c) & (e) and CPCI-NP (d) & (f). The results were expressed as the mean±s.d., n = 3. The temperature was monitored by a thermal camera after laser irradiation (808 nm, 0.8 W cm^{-2}, 30 s).

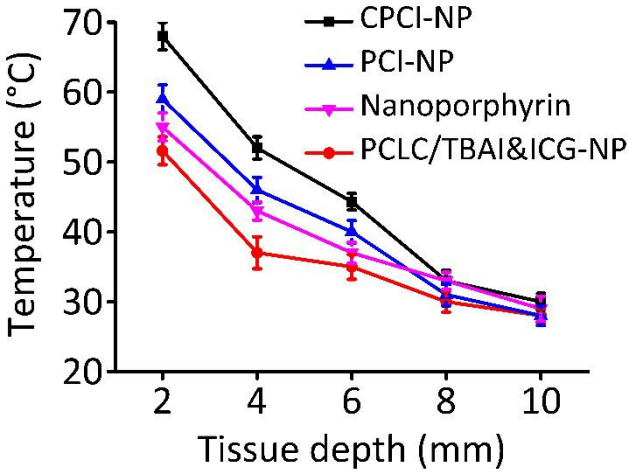

Figure S7. Temperature variation of CPCI-NP, PCI-NP, PCLC/TBAI&ICG-NP and Nanoporphyrin under laser irradiation for 30 s to investigate penetration depth and thermal effect. (Laser: 808 nm, 0.8 W cm^{-2} for CPCI-NP, PCI-NP and PCLC/TBAI&ICG-NP; 690 nm, 0.8 W cm^{-2} for Nanoporphyrin. Nanoporphyrin based on our lab's PEG^{5k}-$Porphyrin_4$-CA_4 telodendrimer)

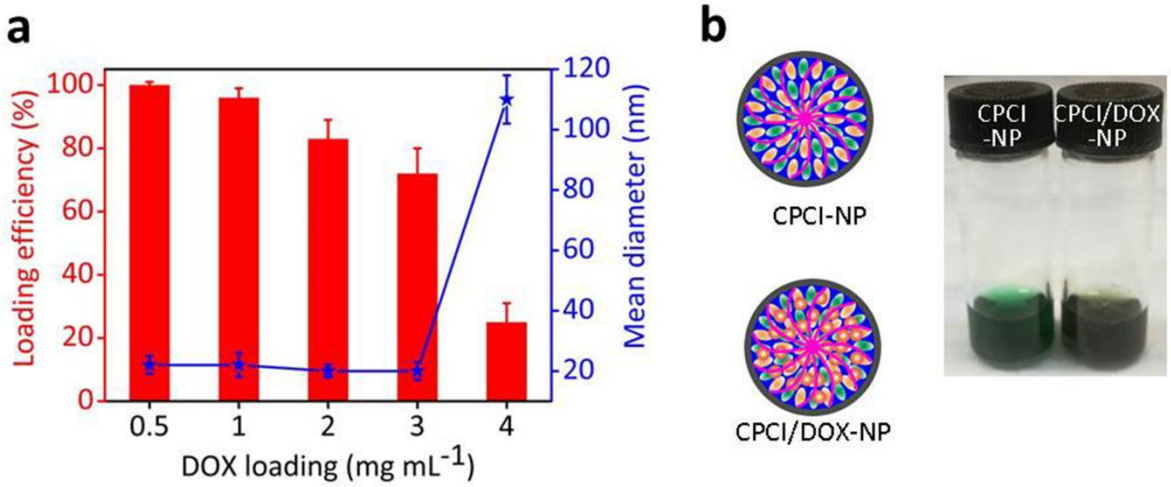

Figure S8. (a) The encapsulation efficiency of DOX into CPCI-NP and size change of CPCI/DOX-NP versus the level of drug-loading. The encapsulation efficiency is defined as the ratio of drug loaded into nanoparticles to the initial drug content. The volume of the final solution was kept at 1 mL and the final concentration of the telodendrimer was 20 mg mL^{-1}. (b) Schematic

illustration and representative photo of CPCI-NP and CPCI/DOX-NP in PBS solution (total telodendrimer concentration: 20 mg mL^{-1}; DOX concentration: 1 mg mL^{-1}).

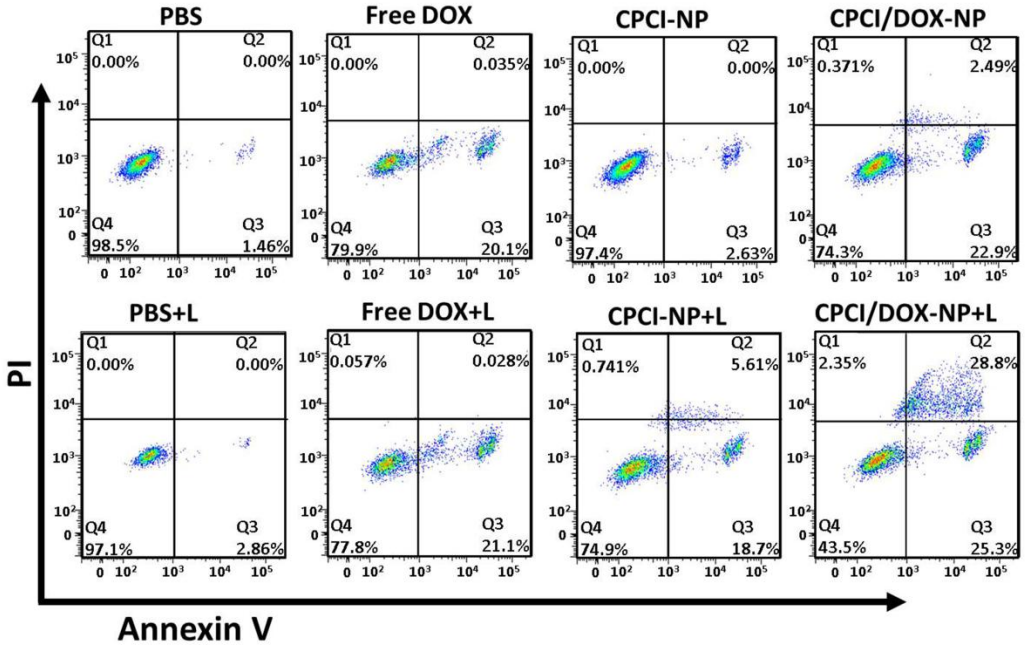

Figure S9. Detection of apoptotic OSC-3 oral cells using Annexin V-FITC and PI flow cytometry assay at various cell culture conditions. Q1: necrotic cells; Q2: late stage apoptotic cells; Q3: normal viable cells; Q4: early stage apoptotic cells. DOX dose: 0.005 mg mL^{-1}; 808 nm laser irradiation: 0.8 W cm^{-2}, 2 min.

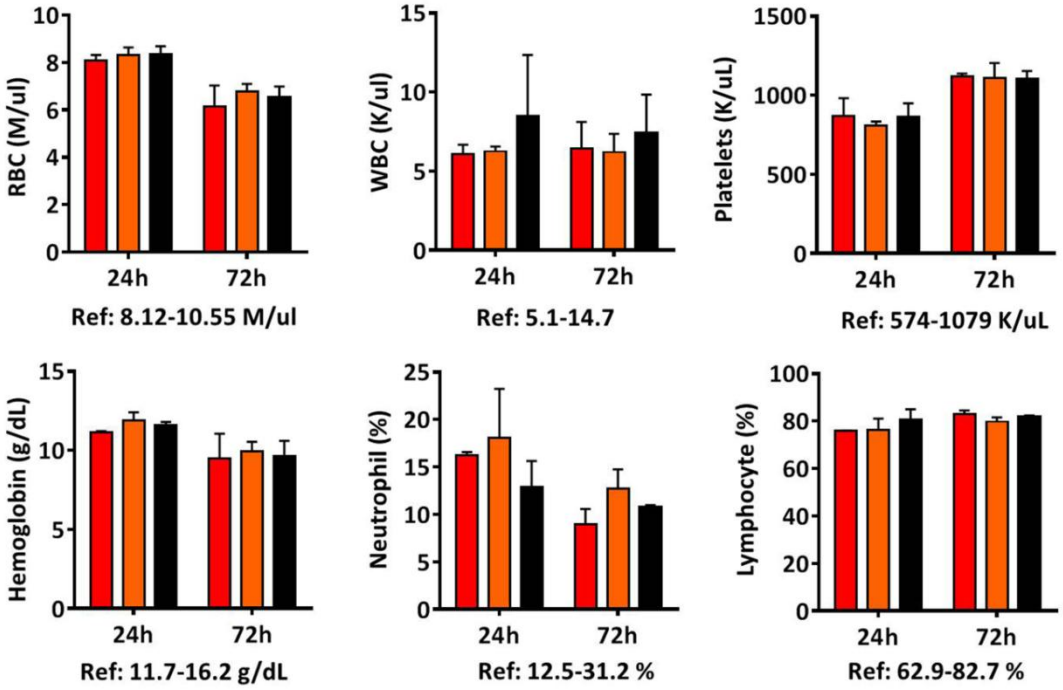

Figure S10. Blood test parameters in terms of RBC, white blood cells (WBC), platelets, hemoglobin, neutrophil and lymphocyte of healthy Balb/c mice intravenously injected with three different concentrations CPCI-NP for 24 h and 72 h (Red: 50 mg kg^{-1}; Orange: 100 mg kg^{-1}; Black: 200 mg kg^{-1}).

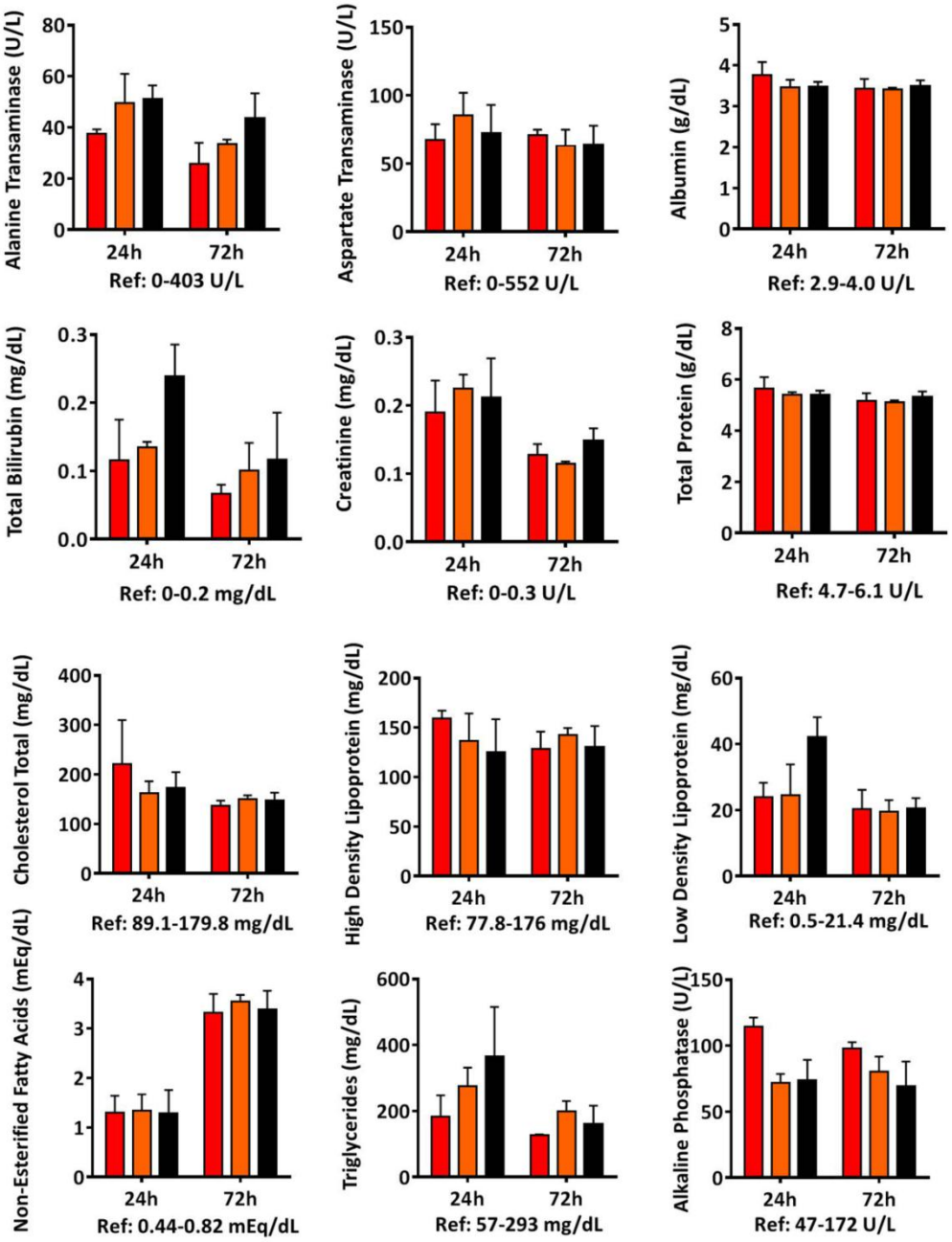

Figure S11. Blood test parameters in terms of liver function alanine aminotransferase, aspartate transaminase, albumin, alkaline phosphatase, aspartic acid transaminase, blood urea nitrogen, creatinine, total bilirubin, creatinine, total protein, total cholesterol, high density lipoprotein, low density lipoprotein, fatty acids, triglycerides and alkaline phosphatase of healthy Balb/c mice intravenously injected with three different concentrations CPCI-NP for 24 h and 72 h (Red: 50 mg kg^{-1}; Orange: 100 mg kg^{-1}; Black: 200 mg kg^{-1}).

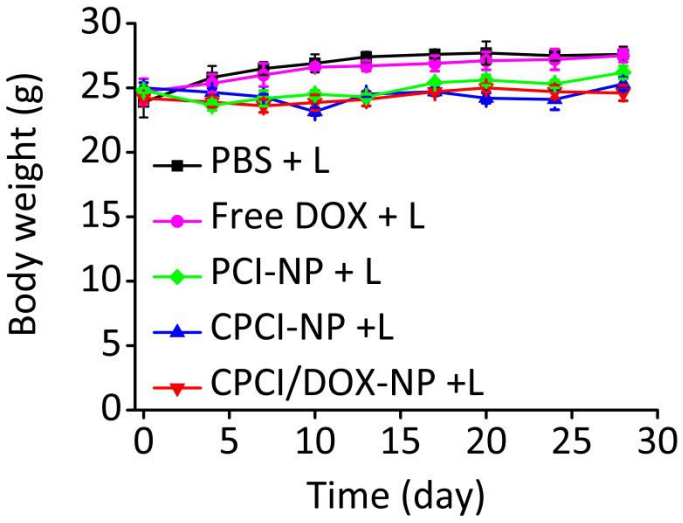

Figure S12. Body weight curves of the experimental mice bearing orthotopic OSC-3 oral cancer receiving different therapeutic formulations *via* tail vein at an interval of 28 days (n = 5; DOX dose: 2.5 mg kg^{-1} and ICGD dose: 7 mg kg^{-1}; data were mean±s.d.).

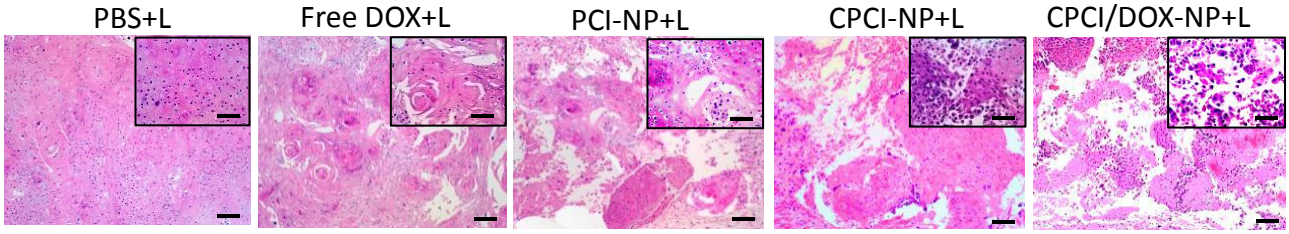

Figure S13. Histological H&E staining of tumor slices after one cycle treatment of orthotopic OSC-3 oral cancer (scale bar = 50 μm in ×100 figures and scale bar = 10 μm in ×400 figures). Dose of DOX: 2.5 mg kg^{-1} and ICGD: 7 mg kg^{-1}.

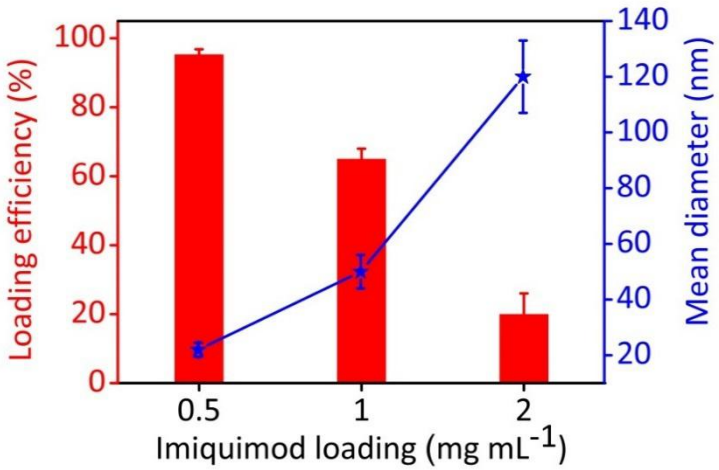

Figure S14. The encapsulation efficiency of imiquimod into CPCI-NP and size change of CPCI/Imiquimod-NP versus the level of drug-loading. The encapsulation efficiency is defined as the ratio of drug loaded into nanoparticles to the initial drug content. The volume of the final solution was kept at 1 mL and the final concentration of the telodendrimer was 20 mg mL^{-1}.

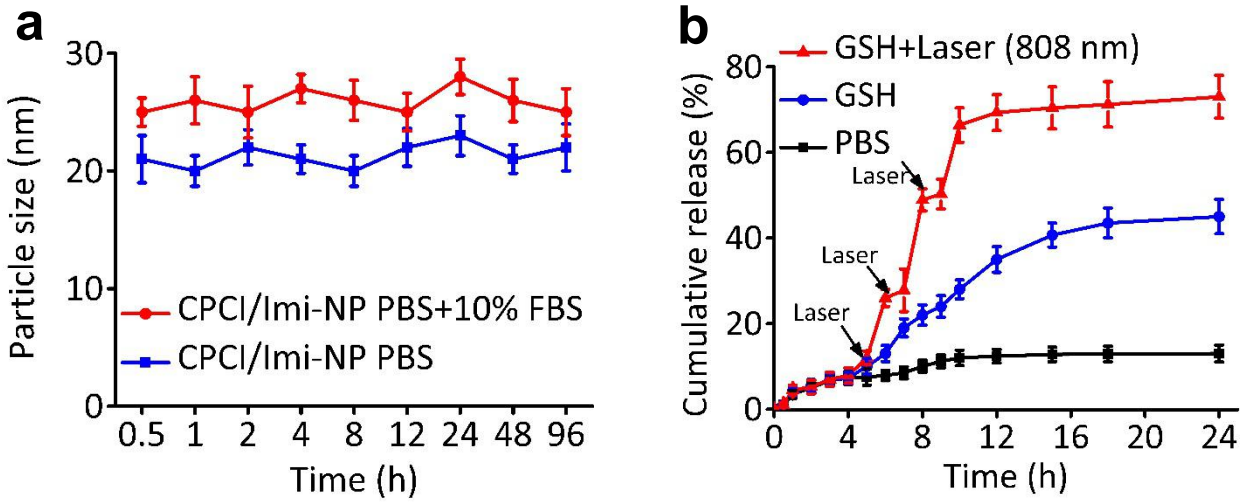

Figure S15. (a) Serum stability of CPCI/imiquimod-NP in PBS solution of pH 7.4 with/without 10% FBS was measured by dynamic light scattering (incubation temperature: 37 °C; data were mean±s.d., n = 3). (b) *In vitro* quantitative imiquimod release of CPCI/imiquimod-NP aqueous solution at PBS, GSH (10 mM) and laser (3 times, 2 min each) plus GSH (10 mM) (Data were mean±s.d., n = 3).

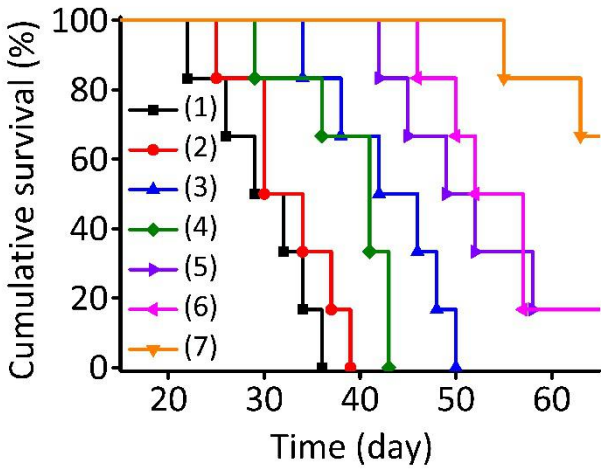

Figure S16. Cumulative survival of different groups of mice (n = 6 per group) with inoculation of 4T1 tumors. Group (1): PBS; Group (2): CPCI/Imiquimod-NP; Group (3): CPCI/Imiquimod-NP plus lase irradiation; Group (4): CPCI-NP plus lase irradiation; Group (5): CPCI/Imiquimod-NP plus anti-PD-1; Group (6): CPCI/Imiquimod-NP plus lase irradiation plus anti-PD-1 (1 cycle); Group (7): CPCI/Imiquimod-NP plus lase irradiation plus anti-PD-1 (2 cycle).

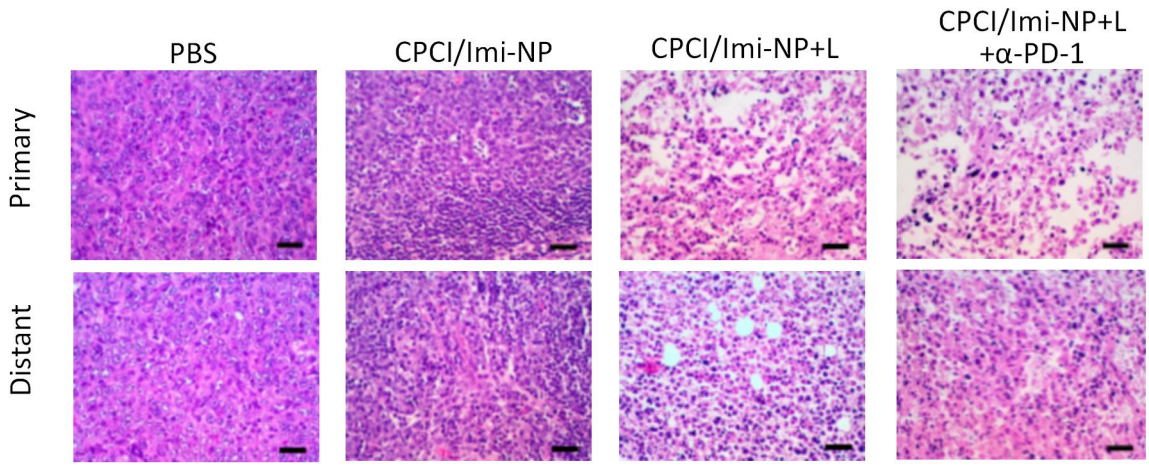

Figure S17. H&E-stained tumor slices collected from mice bearing 4T1 cancer post various treatments (Scale bar = 50 μm).

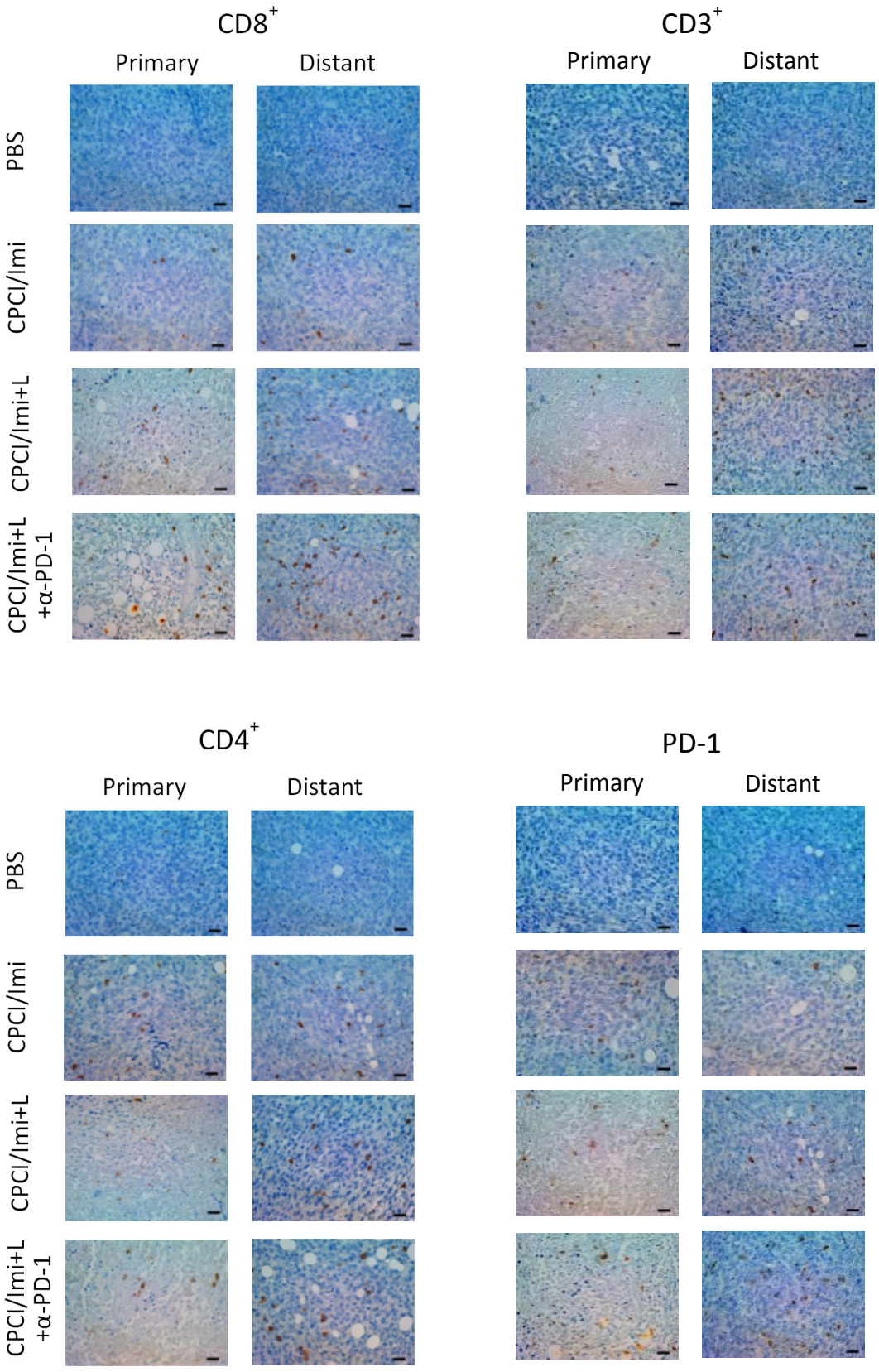
CD8+
Primary
Distant
CD3+
Primary
Distant
PBS
CPCI/Imi
CPCI/Imi+L
CPCI/Imi+L +α-PD-1
CD4+
Primary
Distant
PD-1
Primary
Distant
PBS
CPCI/Imi
CPCI/Imi+L
CPCI/Imi+L +α-PD-1

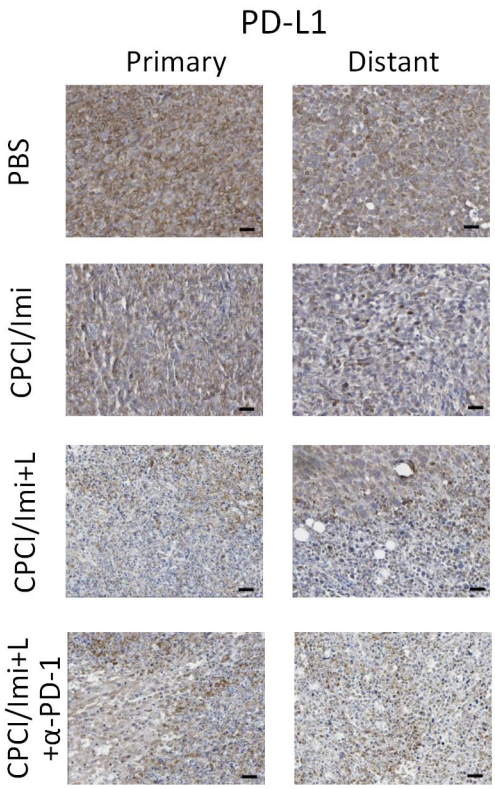

Figure S18. IHC staining for $CD8^+$, $CD3^+$, $CD4^+$, PD-1 and PD-L1 in both sides 4T1 tumor tissue, collected in different treatments (Scale bar = 50 μm).

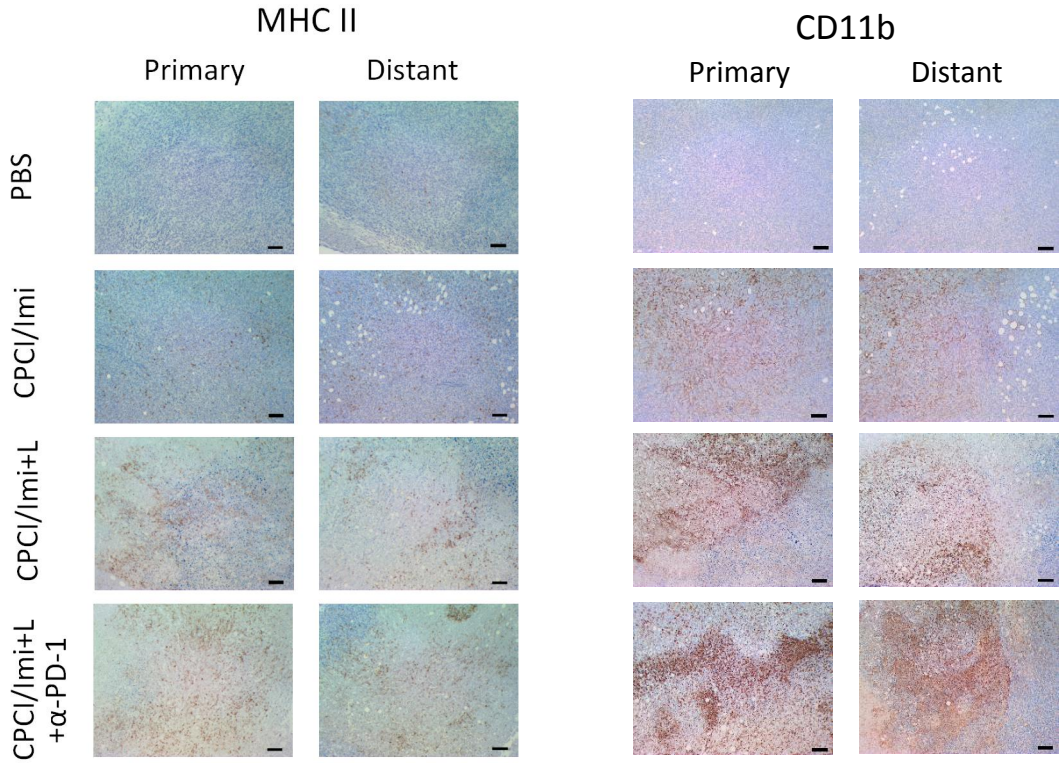

Figure S19. IHC staining for MHC II and CD11b in both sides 4T1 tumor tissue, collected in different treatments (Scale bar = 100 μm).

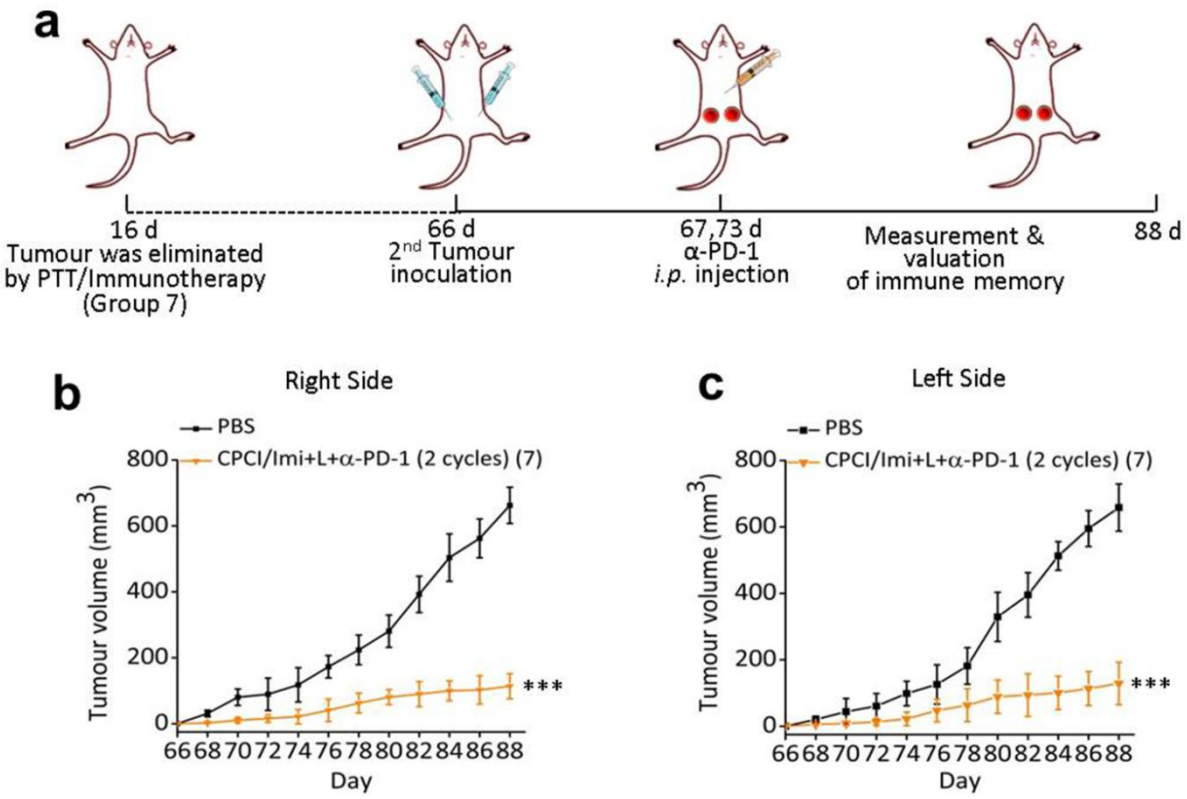

Figure S20. Immune memory effect of synergistic photothermal-/immunotherapy. (a) Schematic illustration of immune-memory by inhibiting cancer relapses at primary and distant sites. (b) Primary tumor and (c) distant tumor growth curves of rechallenged tumors inoculated 50 days post eliminated of their first tumors (intraperitoneal injection of α-PD-1 200 μg per mouse on day 67 and 73); ***$p < 0.001$ in (b) and (c) by comparing PBS control. The previously successfully treated mice were from group 7 mice shown in Figure 5. They were treated with two cycles of CPCI/Imiquimod-NP + 808 nm laser + α-PD-1.

Table S1. Pharmacokinetics parameter in rats received CPCI-NP, PCLC/TBAI&ICG-NP and free ICG (dose of ICG or ICGD is 5mg/kg).

Parameter	Units	CPCI-NP	PCLC/TBAI&ICG-NP	free ICG
$t_{1/2}$	h	41.098 ± 13.443	28.421 ± 16.941	0.087 ± 0.035
AUC(0-t)	mg/L*h	1196.274 ± 91.316	677.571 ± 105.832	12.091 ± 3.295
AUC(0-∞)	mg/L*h	2022.096 ± 282.541	972.914 ± 355.317	15.086 ± 3.469
Vd	L/kg	0.144 ± 0.033	0.196 ± 0.081	1.181 ± 0.321
CL	L/h/kg	0.002 ± 0.001	0.006 ± 0.002	0.436 ± 0.126
Cmax	mg/L	50.078 ± 1.956	35.609 ± 1.836	1.718 ± 0.352